Damir Žarko, Drago Ban, Ratko Klarić

Finite Element Approach to Calculation of Parameters of an Interior Permanent Magnet Motor

A method for calculation of parameters of an interior permanent magnet (IPM) motor at any operating point using 2-D finite element method is presented. This approach is suited to be used in the design stage where it is necessary to determine the motor parameters, namely inductances, which are simultaneously a function on motor dimensions and terminal voltage constraints. An analytical technique based on a 3-D geometric model of the end winding region in which each coil is modeled as a set of serially connected straight filaments has been used for calculation of the end winding leakage inductance. The calculation of the mutual inductance of the end coils is based on the multiple solutions of the Neumann integral. This approach to calculation of motor parameters has been applied in the design of a 1.65 kW IPM motor for which a prototype has been built and tested.

Key words: permanent magnet motor, inductances, finite element method, simulation, testing

1 INTRODUCTION

Interior PM motors are attractive for applications where operation in a wide speed range is required (e.g. traction). Unlike surface PM motors which have the same value of inductance in d and q axes and where all the torque is produced by the magnet flux, interior PM motors have different d and q inductances which results in an additional torque component called reluctance torque. The fundamental torque equation can be derived from the phasor diagram shown in Figure 1 and is given by

$$T_{em} = \frac{3}{2} p \left[\underbrace{\Psi_{md} I_{qs}}_{\substack{\text{Electromagnetic} \\ \text{torque}}} - \underbrace{(L_q - L_d) I_{qs} I_{ds}}_{\substack{\text{Reluctance} \\ \text{torque}}} \right], \quad L_q > L_d$$

(1)

where p is the number of pole pairs, Ψ_{md} is the magnet flux, L_d, L_q, I_{ds} and I_{qs} are the d and q axis inductances and currents respectively. The maximum torque in this case will occur when the current phasor is shifted by an angle γ relative to the q axis. In surface PM motors the maximum torque occurs at $\gamma = 0$, i.e. when the current vector is located in the q axis.

There are two distinct regimes of operation of an IPM motor: constant torque below corner speed and constant power above corner speed, as indicat-
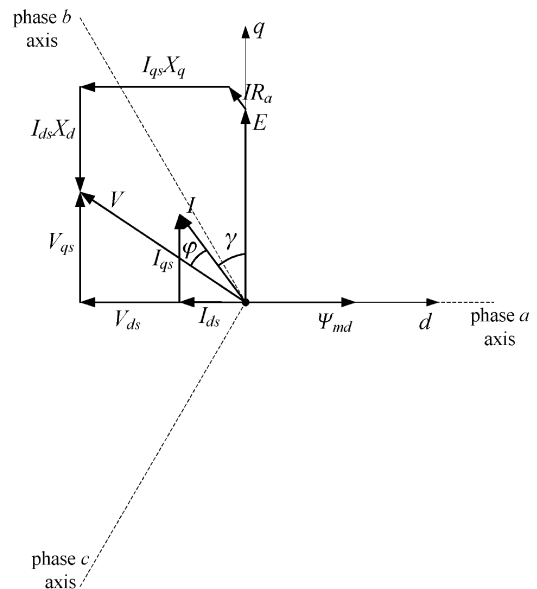

Fig. 1 Phasor diagram of an interior PM motor

ed in Figure 2. The corner speed is defined as the maximum speed at which rated torque can be developed with rated current flowing without exceeding the maximum terminal voltage available from the inverter. Above that speed it is possible to maintain constant power, but it is not possible to develop rated torque without exceeding the voltage
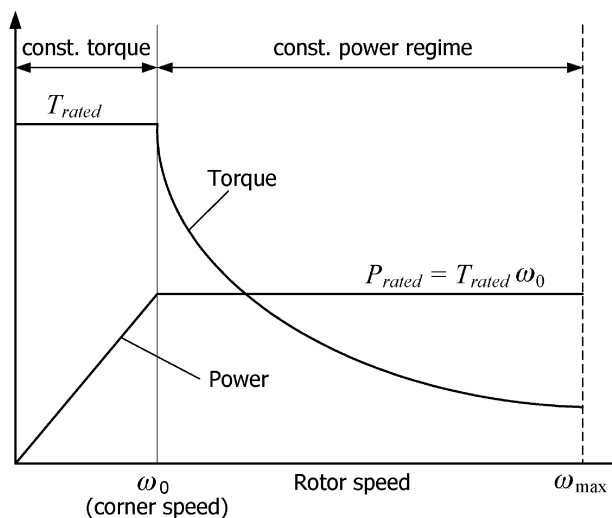
Fig. 2 Capability curves of an interior PM motor

constraint imposed by the power supply. Moreover, the ability to maintain constant power is not universally attainable for all interior PM motor designs. Only designs which satisfy the optimal flux weakening condition first derived by Schiferl and Lipo [1] will give the maximum constant power output in the field weakening regime above corner speed. This condition is given by

$$\Psi_{md} = L_d I_R \qquad (2)$$

where Ψ_{md} is the flux of the magnets alone linked by the armature winding, L_d is the d axis inductance and I_R is the rated armature current. The normalized characteristic current is the quantity used to show the properties of the IPM motor in the flux weakening regime with respect to the optimal flux weakening condition. It is defined as

$$I_c = \frac{\Psi_{md}}{L_d I_R}. \qquad (3)$$

The IPM motor design which satisfies (2) apparently has $I_c = 1$.

The important design parameters of the IPM motor are its inductances, and the magnet flux linkage, since they greatly affect the amount of torque the motor can develop and its power output in the flux weakening regime above corner speed. The calculation of parameters presented in this paper is based on finite element method (FEM) with »permeance freezing« which allows one to use superposition to extract individual parameters of the motor under load and preserve information about saturation while taking into account the effect of cross--saturation as well. This principle has been mentioned previously in literature [2] in the case of

IPM motors, but is also used for calculation of parameters of large synchronous generators [3, 4]. The parameters calculated in this paper refer to the steady state operation. However, FEM can also be used to calculate instantaneous parameters to be used in dynamic models of IPM motors [5, 6].

The main feature of the approach presented in this paper is its suitability for repetitive calculations in the design stage because it allows one to extract information about the motor inductances, the number of turns per coil and the rated current and torque from magnetostatic finite element simulations while taking into account the terminal voltage constraints. For the purpose of motor design, the steady state parameters are in most cases sufficient. This principle of parameter calculation has been integrated into an optimization scheme used to design a 1.65 kW prototype IPM motor which has been built and tested.

2 CALCULATION OF IPM MOTOR PARAMETERS

The proposed IPM motor topology analyzed in this paper is shown in Figure 3. The motor has two layers of cavities in the rotor which are shaped to accommodate magnets of a simple rectangular shape which are cheap to manufacture. The motor has been designed using Differential Evolution optimization algorithm [6] combined with the finite element method. The FEM was used to calculate the motor parameters for each design that emerged out of the optimization scheme. The design objectives were to maximize the electromagnetic torque at corner speed and maximize the characteristic cur-
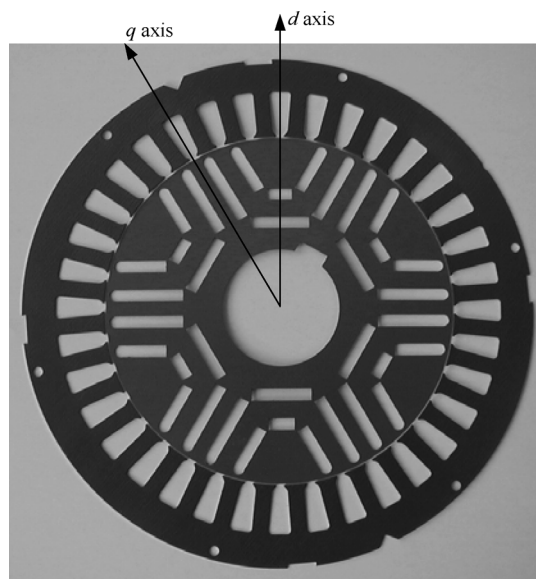

Fig. 3 Stator and rotor laminations of the prototype IPM motor

rent of the motor. The optimization has been formulated as a constrained multiobjective minimization problem where a population of nondominant solutions is determined from which a single solution is selected as the best compromise [8]. The details of the optimization scheme used to design the prototype IPM motor can be found in [9]. Here we only present the results related to calculation of the motor parameters.

To simulate the operating point at the corner speed, a magnitude of the current vector I and its position with respect to the q axis (angle γ) need to be determined first. These two parameters are at the same time constrained by the rated terminal voltage, which in this case is $V_{ll} = 230$ V (line-to-line value). The parameters which are known are the armature current density J and the slot fill factor f_{fill}. They are used to calculate the available number of ampere-turns per slot which follows from

$$N_c I = J S f_{fill} \qquad (4)$$

where N_c is the number of turns per coil and S is the surface area of the slot. The slot area is calculated from the slot dimensions which result from the stator outer and inner diameters and the yoke and tooth thicknesses.

The number of turns per coil and the current need to be separated. The separation can be done in a straightforward manner using a phasor diagram and considering the fact that the sum of the motor back emf and the voltage drops on the armature resistance and inductance have to be equal to the terminal voltage V. The phasor diagram for the interior PM motor is shown in Figure 1. The steady state equations after resolving voltages and currents into d and q components can be written in the general form

$$V_{qs} = R_a I_{qs} + \omega \Psi_{ds}$$
$$V_{ds} = R_a I_{ds} - \omega \Psi_{qs} \qquad (5)$$
$$V = \sqrt{V_{qs}^2 + V_{ds}^2}$$

where

$$\Psi_{qs} = \Psi_{mqd} + L_q I_{qs} + L_{qd} I_{ds}$$
$$\Psi_{ds} = \Psi_{md} + L_d I_{ds} + L_{dq} I_{qs}. \qquad (6)$$

Equations (6) also include the cross saturation terms which will be further discussed in the paper. The motor is designed for a rated operating point at corner speed (1000 rpm). The parameters are initially calculated with an assumption that there is only one turn per coil with $N_c I$ as the total current in the coil. The available number of ampere turns per coil $N_c I$ is obtained from (4). The additional problem with the IPM motor is the lack of knowledge about the current control angle γ_{Tmax} (see
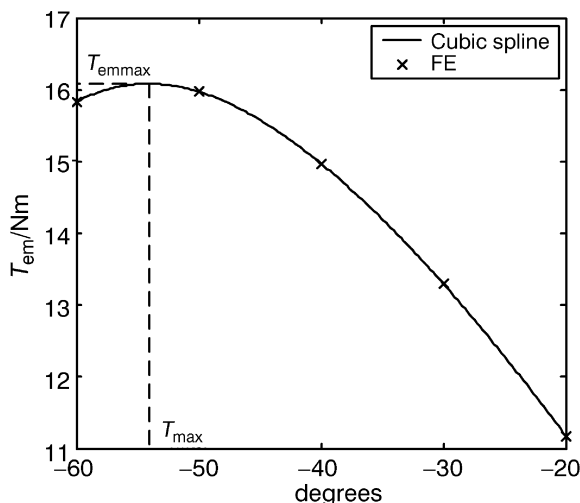

Fig. 4 Torque versus control angle curve used to find the control angle for maximum torque. Cubic spline is used to generate the curve from five points obtained by FE method

Figure 4) at which maximum torque is achieved with rated armature current flowing. The rated current is defined as the maximum rms current at corner speed at which the maximum temperature in the armature winding will not exceed the value allowed by the class of insulation assuming continuous operation of the motor. To determine γ_{Tmax}, five nonlinear magnetostatic FE simulations with γ ranging from $-20°$ to $-60°$ are run first. The electromagnetic torque is calculated for each value of γ using the well known equation

$$T_{em} = \frac{3}{2} p (\Psi_{ds} I_{qs} - \Psi_{qs} I_{ds}) \qquad (7)$$

where p is the number of pole pairs, Ψ_{ds}, Ψ_{qs}, I_{ds} and I_{qs} are the d and q components of the flux linkage and current respectively. The flux linkages Ψ_{ds} and Ψ_{qs} are determined from the flux linkages of phases a, b and c. For instance, the phase a flux linkage is calculated as a sum of the flux linkages of all phase a coils. The flux linkage of each individual coil is equal to the line integral of the magnetic vector potential A_z along the contour of the coil. In a 2-D FE model this integral is proportional to the difference between the average potentials in the meshed geometric regions occupied by the coil sides located in different pole regions. The phase a flux linkage is then

$$\Psi_a = p \sum_{k=1}^{Q_{coil\,p}} \Psi_{coilk} =$$

$$= p \sum_{k=1}^{Q_{coil\,p}} \frac{1}{S} \left(\int_{S_1} A_z \mathrm{d}S - \int_{S_2} A_z \mathrm{d}S \right) N_c l_a \qquad (8)$$

where $Q_{\mathrm{coil}p}$ is the number of coil sides per phase in one pole region, p is the number of pole pairs, N_c is the number of turns of each coil, l_a is the length of the stator core and S is the cross-section of the coil region. Subscripts 1 and 2 denote coil sides located in different pole regions. Since the number of turns per coil is not known at this stage, the flux linkages Ψ_{a0}, Ψ_{b0} and Ψ_{c0} are calculated assuming $N_c = 1$. The flux vector can now be formed

$$\underline{\Psi}_0 = \Psi_{ds0} + j\Psi_{qs0} = \frac{2}{3}(\Psi_{a0} + a\Psi_{b0} + a^2\Psi_{c0}),$$
$$a = e^{j\frac{2\pi}{3}} \tag{9}$$

with

$$\Psi_{ds0} = \frac{2}{3}\left(\Psi_{a0} - \frac{1}{2}\Psi_{b0} - \frac{1}{2}\Psi_{c0}\right)$$
$$\Psi_{qs0} = \frac{1}{\sqrt{3}}(\Psi_{b0} - \Psi_{c0}). \tag{10}$$

The subscript 0 is used to emphasize the fact that flux linkages are calculated with $N_c = 1$. The currents I_{qs} and I_{ds} are also not known, but the total ampere turns per slot N_cI are known from (4). Using γ and N_cI one can calculate

$$N_cI_{qs} = N_cI \cos\gamma$$
$$N_cI_{ds} = N_cI \sin\gamma. \tag{11}$$

Considering the fact that $\Psi_{ds} = N_c\Psi_{ds0}$ and $\Psi_{qs} = N_c\Psi_{qs0}$, the torque equation (7) can be written in the form

$$T_{em} = \frac{3}{2}p(\Psi_{ds0}N_cI_{qs} - \Psi_{qs0}N_cI_{ds}) \tag{12}$$

where N_cI_{qs} and N_cI_{ds} are calculated from (11). With the torque calculated for five values of γ, cubic spline is used to generate a smooth T_{em} vs. γ curve as shown in Figure 4 and find the value of $T_{\max}$ where the maximum torque occurs.

Another nonlinear simulation with $\gamma_{T\max}$ as the control angle is run to get the field solution for this operating point. The flux lines and the distribution of permeabilities for the rated operating point at corner speed are shown in Figures 5 and 6 respectively. The most effective approach to calculate saturated L_d, L_q and Ψ_{md} at this operating point and still preserve all the information about the saturation in the motor is to »freeze« the permeabilities in the nodes of the finite element mesh. Once the permeabilities are frozen the problem becomes linear and the parameters can be determined one at the time. Three linear magnetostatic simulations are needed to determine L_d, L_q and Ψ_{md}. In addition, cross-saturation parameters L_{qd}, L_{dq} and Ψ_{mqd} can be determined from the same simulations. Al-
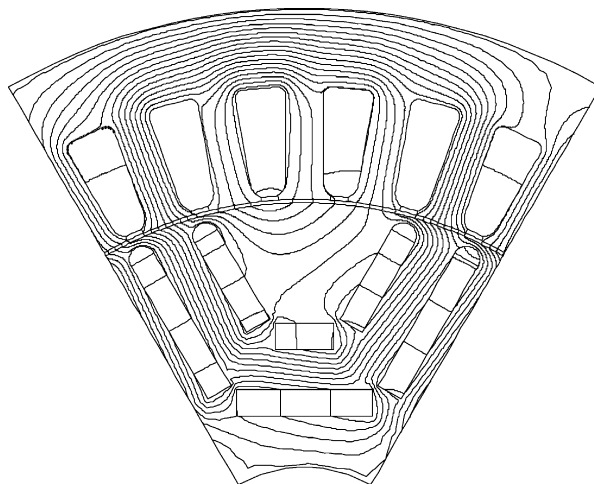

Fig. 5 Flux lines in the cross section of the prototype IPM motor for the case of rated torque at corner speed of 1000 rpm
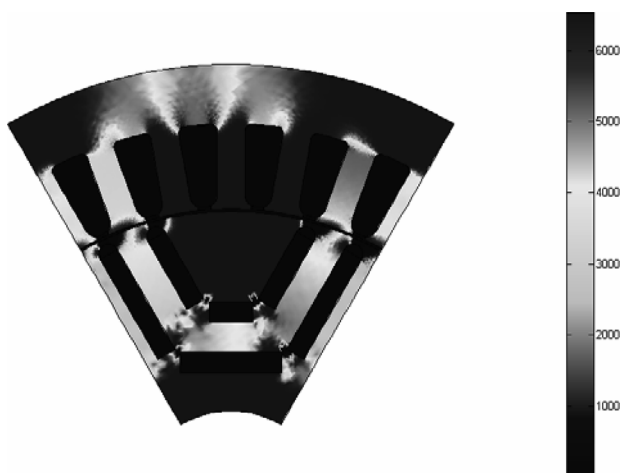

Fig. 6 Distribution of relative permeabilities in the cross section of the prototype IPM motor for the case of rated torque at corner speed of 1000 rpm

though small in this particular case, the effect of cross-saturation has been generally recognized as the phenomenon caused by saturation which manifests itself as the flux linkage in the axis perpendicular to the axis where the excitation is applied. At this stage the inductances will be calculated for $N_c = 1$ since the actual N_c is still unknown.

2.1 Inductances L_{d0} and L_{qd0}

The first linear simulation is used to calculate L_{d0} and L_{qd0}. The magnet flux is turned off by setting the magnet remanence B_r to zero. The current vector must be aligned with the d axis. Since the problem has become linear after freezing the permeabilites, the magnitude of the current vector can be chosen arbitrarily. If the magnitude is chosen to be 1 A, then to align the current vector with the d
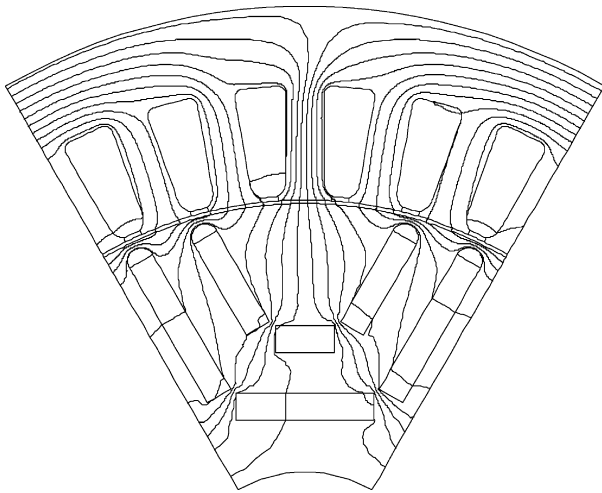
Fig. 7 *Flux lines in the cross section of the prototype IPM motor with frozen permeabilities used for calculation of saturated inductances L_{d0} and L_{qd0}*

axis the instantaneous phase currents have to be defined as

$$i_a = 1\,\text{A}, \ \ i_b = i_c = -\frac{i_a}{2} = -0.5\,\text{A}. \qquad (13)$$

The d and q components of the current vector are then

$$i_{ds} = 1\,\text{A}, \ \ i_{qs} = 0. \qquad (14)$$

Figure 7 shows the field solution for this case. The flux linkages of phases a, b and c are calculated according to (8). The flux vector is formed and its d and q components are calculated using (9) and (10). The inductances for one turn per coil are then

$$L_{d0} = \frac{\Psi_{ds0}}{i_{ds}}, \ \ L_{qd0} = \frac{\Psi_{qs0}}{i_{ds}}. \qquad (15)$$

Inductance L_{d0} only takes into account the flux linkage in the core region. The 2-D FE simulation neglects the leakage flux in the end region. Hence, the end winding leakage inductance L_{ew0} is calculated separately using a 3-D analytical approach described later in this chapter and added to L_{d0} to calculate the total L_d. For the inductance L_{qd0} 2-D FE simulation is sufficient since there is no cross-saturation effect in the end region because the end winding is located in the air.

2.2 Inductances L_{q0} and L_{dq0}

The inductances L_{d0} and L_{dq0} are calculated in a similar manner, only in this case the current vector needs to be aligned with the q axis. The phase currents are then

$$i_a = 0, \ \ i_b = -i_c = \frac{\sqrt{3}}{2}\,\text{A} \qquad (16)$$

which in turns gives

$$i_{ds} = 0, \ \ i_{qs} = 1\,\text{A}. \qquad (17)$$

The field solution is shown in Figure 8. After calculating the flux components, the inductances for one turn per coil are given by

$$L_{q0} = \frac{\Psi_{qs0}}{i_{qs}}, \ \ L_{dq0} = \frac{\Psi_{ds0}}{i_{qs}}. \qquad (18)$$

2.3 Flux linkages Ψ_{md0} and Ψ_{mqd0}

This simulation is used to calculate magnet flux linked by the armature winding. In this case the
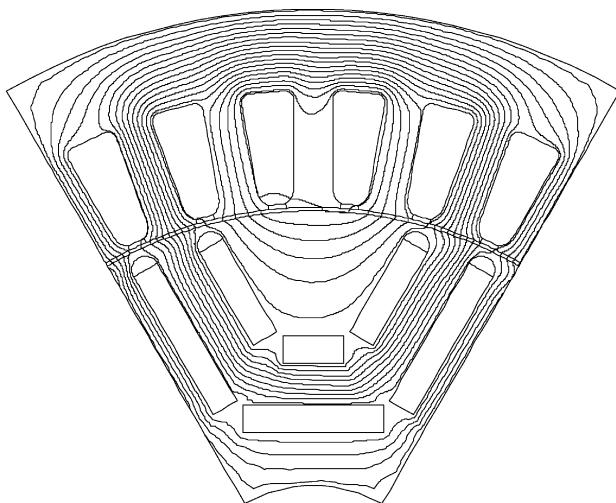

Fig. 8 *Flux lines in the cross section of the prototype IPM motor with frozen permeabilities used for calculation of saturated inductances L_{q0} and L_{dq0}*
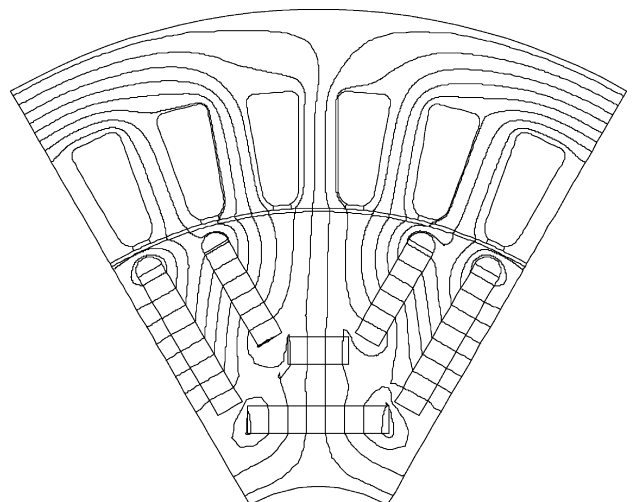

Fig. 9 *Flux lines in the cross section of the prototype IPM motor with frozen permeabilities used for calculation of the flux linkages Ψ_{md0} and Ψ_{mqd0}*

magnets are turned on by setting the magnet rema-nence B_r to the actual value while phase currents are equal to zero. The field solution is shown in Figure 9. The flux linkages of the phase windings are calculated again using the previously described procedure. Equation (10) is then used to calculate the flux linkages Ψ_{md0} and Ψ_{mq0}. Note that although the magnets act only in the direction of the d axis, there will also be a small cross saturation flux link-age in the q axis.

2.4 End winding leakage inductance L_{ew0}

The end winding leakage inductance is a part of the total leakage inductance of the phase winding. In the core region the coils are located in the slots which, with the assumption that iron is infinitely permeable, makes it easier to predict the distribu-tion of the leakage flux and calculate the leakage inductance. The end winding region is more diffi-cult to analyze because its magnetic circuit is en-tirely in the air and its winding structure is often characterized by complex three-dimensional geome-try of the coils. An additional difficulty is the ef-fect that adjacent coils and phases have on each other.

The most accurate approach to the end winding leakage inductance calculation would be to use the 3-D finite element method. The main problem with the 3-D FE method is the fact that the drawing of a complex 3-D geometric structure, mesh genera-tion and solution of a very large system of equa-tions are extremely time consuming. This is the main obstacle for practical utilization of the 3-D FE method for the end winding leakage inductance calculation in the design stage, especially if opti-mization is involved. The analytical approach is the remaining alternative. There are different closed form analytical solutions that can be found in litera-ture [10–12]. One of the major problems of these solutions is that they have been derived for an as-sumed geometric shape of the end coil which may not be applicable for all types of windings and all types of machines with different power ratings. Therefore a more flexible method has been used in this paper which models the end coil as a set of serially connected straight filaments. This allows one to define the end coil geometry of an arbitrary shape and still calculate the inductance in a unique manner.

The mutual inductance between any two coils in the end region is calculated by adding the contri-butions of all possible pairs of filaments in both coils. The method has been described in detail in [13, 14] for the case of a turbogenerator with dou-ble-layer involute winding. It has been modified and adapted in this paper to be used for a single-layer

end winding structure typical for small permanent magnet motors. The method also takes into account the influence of the iron core by applying the method of images. Some assumptions on the mag-netic properties of the core and the geometry of the end region are necessary to simplify the prob-lem. The following assumptions are made:

- the permeability of the iron core is constant,
- the iron core surface extends infinitely and fills the entire half-space,
- the influences of slots, air gap and rotor shaft are neglected,
- the coils are represented by infinitely thin con-ductors.

The three-dimensional contour of the end coil is replaced by an arbitrary number of straight fila-ments depending on the desired accuracy of the geometric model of the coil.

Such model for a single layer overlapping wind-ing of a prototype IPM motor is shown in Figure 10. The complete model of the end winding con-taining all the coils is shown in Figure 11.

Talking about mutual inductance of the end coils is incorrect, because an end coil does not represent a closed circuit. For the lack of a better term, we shall refer to the mutual inductance of the end coils by which we shall imply the contribution to the mutual inductance of the end parts of the coils. Generally, the mutual inductance between two closed infinitely thin contours l_1 and l_2 in space can be calculated as

$$M = \frac{\mu_0}{4\pi I} \oint_{l_1} \frac{\mathrm{d}\vec{l_1}\mathrm{d}\vec{l_2}}{r} \tag{19}$$
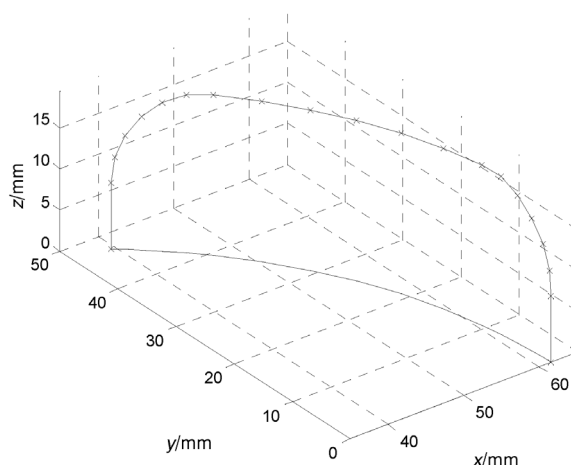

Fig. 10 3-D model of the end coil of a single-layer overlapping winding comprised of 20 straight filaments
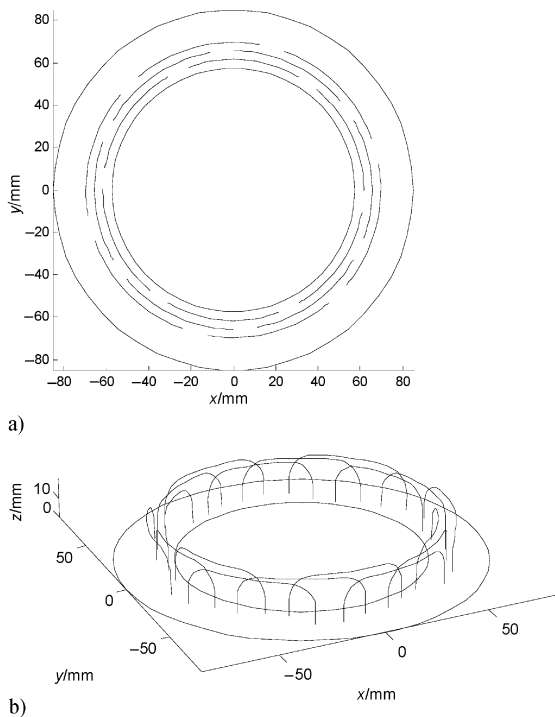
a)

b)

Fig. 11 Full 3-D model of a single-layer overlapping end winding of the six pole prototype IPM motor. a) XY plane, b) Perspective view

where r is the distance between segments $\vec{dl_1}$ and $\vec{dl_2}$. If the contour of the end coil is replaced by a sequence of straight filaments, then (19) is replaced by a sum of integrals of the form (Neumann integrals)

$$N = \cos\varphi \int_A^B dl_1 \int_a^b \frac{dl_2}{r} \qquad (20)$$

which are solved for all possible combinations of straight filaments in both coils. This integral is based on the integration of the magnetic vector potential due to the current in one coil along the contour of the other coil and represents the flux linkage. The angle φ in (20) is the angle between the directional vectors of two straight lines in 3-D space while A, B, a and b denote starting and ending points of each filament. The general solution of the Neumann integral for two straight filaments in an arbitrary position relative to each other in space can be found in [14].

The mutual inductances are calculated between the first coil and all other coils obtained by rotating every subsequent coil by an angle that corresponds to two slot pitches. Thus, the mutual inductance between any two coils amounts to calculation of the mutual inductance of the first coil and another coil shifted by a certain number of slot pitches. The mutual inductance of the coils of one phase is calculated by adding the mutual inductance of the first coil and all the others that belong to the same phase. The obtained result is multiplied by two to take into consideration both sides of the machine. The mutual inductance of two phases contains the sum of mutual inductances of every coil from the first phase and every coil from the second phase. Due to symmetry, the mutual inductances of any two phases are equal. The total inductance per phase is equal to the sum of the self inductance and the mutual inductance with other two phases. With the existence of the parallel paths in the winding, the obtained result is divided by the squared number of paths (a_p^2) because the inductance per phase is proportional to the squared number of turns connected in series.

The mutual inductances between the first coil and all other coils for different values of iron permeability are shown in Figure 12. The curves obtained for $\mu_r = 0$ and $\mu_r = 1$ represent the lower and upper bounds within which one would expect to find the actual value of the end winding inductance. Table 1 contains the values of the end winding leakage inductance calculated for different values of relative permeability of iron. When $\mu_r = 0$, it is assumed that the iron is infinitely conductive and impermeable. When $\mu_r = 1$, the influence of iron is neglected. Finally, when $\mu_r = \infty$, it is assumed that the iron is infinitely permeable and infinitely resistive. For calculation purposes, infinity is replaced by the value of 10^9 for the relative permeability.

In an actual motor, the core, the shaft and the frame would act more as a conductive screen than as a permeable, highly resistive surface. Therefore, it is reasonable to take the value of the end win-
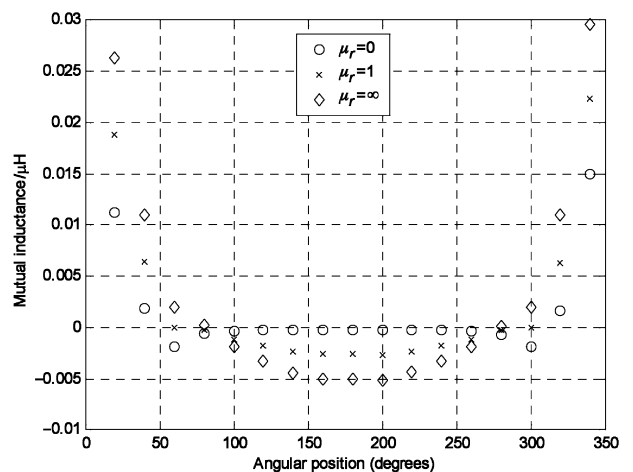

Fig. 12 Mutual inductance between two end coils as a function of relative coil positions for the single-layer winding of the prototype IPM motor assuming one turn per coil

Table 1 **End winding leakage inductance for different values of relative iron permeability and one turn per coil**

Relative permeability of iron core μ_r	Self inductance of one phase L_{sew0}, μH	Mutual inductance between two phases M_{ew0}, μH	Total leakage inductance $L_{ew0}=L_{sew0}+M_{ew0}$ μH
0	0.9625	0.1188	1.0813
1	1.0082	0.1444	1.1527
∞	1.0539	0.1701	1.2240

ding leakage inductance calculated with $\mu_r = 0$ as an actual motor parameter. At this stage the leakage inductance is calculated assuming that $N_c = 1$.

2.4.1 Armature winding resistance R_{a0}

The armature winding resistance is initially also calculated assuming one turn per coil. The cross area of the conductor is calculated from the slot area S and the slot fill factor f_{fill}. The resistance for a single-layer lap winding with one turn per coil is

$$R_{a0} = \frac{1}{\kappa_{75}} \frac{l_{turn}Q_s}{3a_p^2 f_{fill}S} \qquad (21)$$

where l_{turn} is the total length of one coil turn, Q_s is the number of slots, a_p is the number of parallel branches and κ_{75} is the conductivity of copper at 750 °C.

2.4.2 Number of turns per coil and the actual parameters

The relationships between the actual parameters and the ones calculated for one turn per coil are given by

$$R_a = N_c^2 R_{a0}$$
$$L_d = N_c^2 (L_{d0} + L_{ew0})$$
$$L_{qd} = N_c^2 L_{qd0}$$
$$L_q = N_c^2 (L_{q0} + L_{ew0}) \qquad (22)$$
$$L_{dq} = N_c^2 L_{dq0}$$
$$\Psi_{md} = N_c \Psi_{md0}$$
$$\Psi_{mqd} = N_c \Psi_{mqd0}.$$

The number of turns per coil can now be calculated by combining (5), (6) and (22) in the following manner:

Thus the number of turns per coil N_c is uniquely determined from the terminal voltage V and the motor parameters calculated assuming that $N_c = 1$ for the case of rated torque at corner speed. Once the number of turns per coil is known the rated current of the motor is simply

$$I_R = \frac{N_c I}{N_c} \qquad (24)$$

where $N_c I$ is calculated from (4). The inductances, the flux linkages and the number of turns per coil of the prototype IPM motor have been calculated in the proposed manner and are shown in Table 2 together with some other important data of the motor. The correctness of the IPM motor model based on parameters thus calculated can be verified by comparing the electromagnetic torque calculated directly from the FE simulation and calculated from the expression

Table 2 **Parameters of the prototype IPM motor**

Parameter	Symbol	Value
Rated power, W	P	1651
Rated line voltage, V	V	230
Rated current, A	I	7.63
Rated corner speed, rpm	n_r	1000
Maximum speed, rpm	n_{max}	6000
Rated electromagnetic torque, Nm	T_{em}	16.09
Rated shaft torque, Nm	T	15.70
Power factor	$\cos\varphi$	0.628
Efficiency	η	0.887
RMS linear current density, A/m	K_{1s}	20538
Magnet remanence, T	B_r	0.20
Magnet relative permeability	μ_r	1.15
Number of turns per coil	N_c	27
Armature resistance at 75 °C, Ω	R_a	1.01
Saturated q axis inductance at corner speed, mH	L_q	76.1
Saturated d axis inductance at corner speed, mH	L_d	32.4
End winding leakage inductance, mH	L_{ew}	0.788
Saturated saliency ratio	ξ	2.35
Current control angle, deg	γ	−46.83
Cross saturation inductance, mH	L_{dq}	1.039
Cross saturation inductance, mH	L_{qd}	1.039
Magnet flux (rms value), Vs	Ψ_{md}	0.1012
Magnet cross saturation flux (rms value), Vs	Ψ_{mqd}	−0.0017
RMS line-to-line back emf at 6000 rpm, V	E_{max}	160

$$N_c = \frac{V}{\sqrt{\left[R_{a0}N_cI_{ds} - \omega L_{q0}N_cI_{qs} - \omega L_{qd0}N_cI_{ds} - \omega\Psi_{mqd0}\right]^2 + \left[R_{a0}N_cI_{qs} + \omega L_{d0}N_cI_{ds} + \omega L_{dq0}N_cI_{qs} + \omega\Psi_{md0}\right]^2}}. \qquad (23)$$

$$T_{em} = 3p(\Psi_{ds}I_{qs} - \Psi_{qs}I_{ds}) \qquad (25)$$

with d and q flux and current components given as rms values. After taking into account that

$$\Psi_{qs} = \Psi_{mqd} + L_q I_{qs} + L_{qd} I_{ds}$$
$$\Psi_{ds} = \Psi_{md} + L_d I_{ds} + L_{dq} I_{qs} \qquad (26)$$
$$L_{dq} = L_{qd}, \ I_{qs} = I\cos\gamma, \ I_{ds} = I\sin\gamma$$

and substituting into (25), the torque equation takes the form

$$T_{em} = 3p\Big[\Psi_{md}I_{qs} - \Psi_{mqd}I_{ds} + (L_d - L_q)I_{ds}I_{qs} +$$
$$+ L_{dq}(I_{qs}^2 - I_{ds}^2)\Big] =$$
$$= 3p\Big[\Psi_{md}I\cos\gamma - \Psi_{mqd}I\sin\gamma + \qquad (27)$$
$$+ \frac{1}{2}(L_d - L_q)I^2\sin(2\gamma) + L_{dq}I^2\cos(2\gamma)\Big].$$

The torque calculated using (27) with parameters from Table 2 is

$$T_{em} = 3\cdot3\cdot\Big[0.1012\cdot7.63\cdot\cos(-46.83°) -$$
$$-(-0.0017)\cdot7.63\cdot\sin(-46.83°) +$$
$$+\frac{1}{2}(0.0761 - 0.0324)7.63^2\cdot\sin(-2\cdot46.83°) + \qquad (28)$$
$$+ 0.001039\cdot7.63^2\cos(-2\cdot46.83^2)\Big] = 16.13 \text{ Nm}$$

which is very close to 16.09 Nm in Table 2 calculated directly from the FE solution.

3 COMPARISON OF CALCULATED AND MEASURED INDUCTANCES

The 1.65 kW prototype IPM motor has been designed using the multiobjective optimization algorithm previously mentioned. The IPM motor cou-
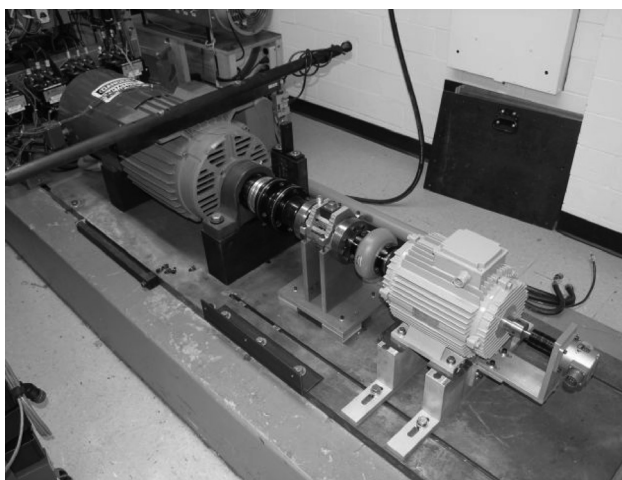

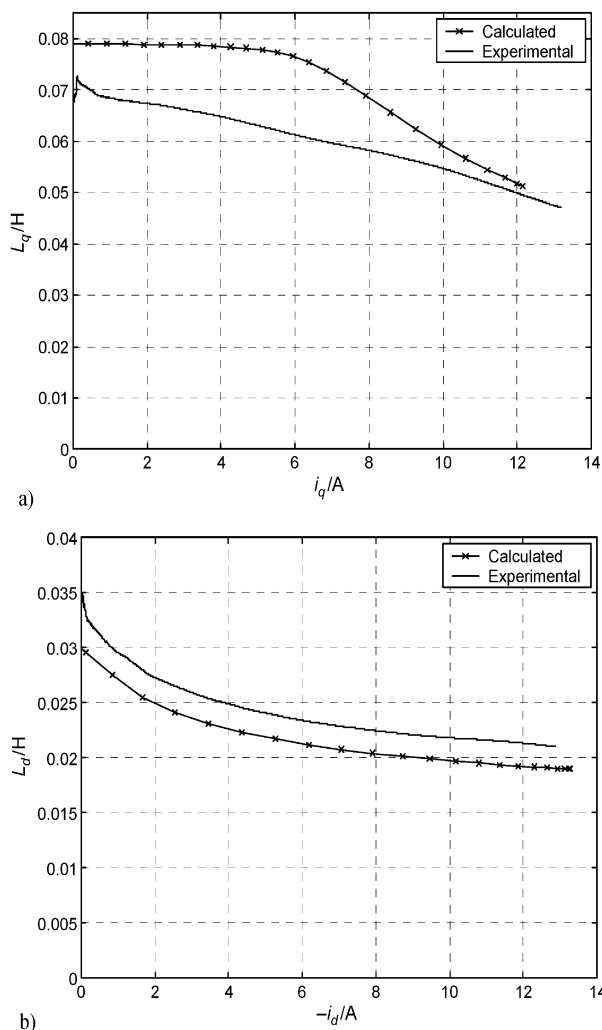*Fig. 13 Prototype IPM motor coupled to the induction machine via torque transducer*

Fig. 14 Comparison of measured and calculated inductances of the prototype IPM motor; a) q axis inductance, b) d axis inductance

pled to a 25 kW induction machine which is used as a load is shown in Figure 13. The purpose of designing and building the prototype has been to investigate if the physical properties of the motor predicted in the design stage can be actually achieved in practice. The armature winding inductances L_d and L_q have been measured using static tests with the locked rotor. The results of experiments conducted on the motor showed that the measured q axis inductance was approximately 10–20 % lower than the calculated one, while the measured d axis inductance was about 10 % higher than calculated (Figures 14a and 14b). The lower value of the inductance L_q could be attributed to a larger effective air gap than assumed by the design. The larger air gap can occur due to manufacturing imperfections, but can also be created by changed properties of the core material due to punching and laser cutting of the rotor laminations.

4 CONCLUSIONS

A finite element based approach to calculation of inductances of an interior PM motor has been presented. This particular approach is suitable to be used in the design stage since it allows one to calculate the motor parameters while simultaneously taking into account the terminal voltage constraint at the corner speed. Thus it is possible to determine the number of turns per coil and the rated armature current from a single magnetostatic FE simulation. This principle of parameter calculation has been integrated into an optimization scheme used to design the 1.65 kW prototype IPM motor which has been built and tested. The difference between calculated and measured inductances of the prototype motor is between 10 % and 20 %. Such difference could be attributed to manufacturing imperfections or changed properties of the core material due to punching of the stator laminations and laser cutting of the rotor laminations.

REFERENCES

[1] R. F. Schiferl, T. A. Lipo, **Power Capability of Salient Pole Permanent Magnet Synchronous Motors in Variable Speed Drive Applications.** IEEE Trans. on Industry Applications, Vol. 26, pp. 115–123, Jan./Feb. 1990.

[2] N. Bianchi, S. Bolognani, **Magnetic Models of Saturated Interior Permanent Magnet Motors Based on Finite Element Analysis.** Thirty-Third IAS Annual Meeting, St. Louis, Missouri, Vol. 1, pp. 27–34, 12-15 Oct 1998.

[3] K. Ide, S. Wakui, K. Shima, M. Takahashi, K. Miyakawa, Y. Yagi, **Analysis of Saturated Synchronous Reactances of Large Turbine Generator by Considering Cross-Magnetizing Reactances Using Finite Elements.** IEEE Trans. on Energy Conversion, Vol. 14, No. 1, March 1999.

[4] M. A. Arjona L., D. C. Macdonald, **A New Lumped Steady--State Synchronous Machine Model Derived from Finite Element Analysis.** IEEE Trans. on Energy Conversion, Vol. 14, No. 1, March 1999.

[5] B. Štumberger, G. Štumberger, D. Dolinar, A. Hamler, M. Trlep, **Evaluation of Saturation and Cross-Magnetization Effects in Interior Permanent-Magnet Synchronous Motor.** IEEE Trans. on Industry Applications, Vol. 39, No. 5, Sept./Oct. 2003.

[6] L. Chedot, G. Friedrich, **A Cross Saturation Model for Interior Permanent Magnet Synchronous Machine.** Application to a Starter-Generator. 39th IAS Annual Meeting, Vol. 1, pp. -70, Seattle, USA, 3–7 Oct. 2004.

[7] R. Storn, K. Price, **Differential Evolution – a Simple and Efficient Adaptive Scheme for Global Optimization over Continuous Spaces.** Technical Report TR-95-012, ICSI, March 1995.

[8] C. A. C. Coello, R. L. Becerra, **Evolutionary Multi-objective Optimization Using a Cultural Algorithm.** Proceedings of the 2003 IEEE Swarm Intelligence Symposium, pp. 6–13, April 2003.

[9] D. Žarko, **A Systematic Approach to Optimized Design of Permanent Magnet Motors With Reduced Torque Pulsations.** Ph.D. thesis, University of Wisconsin-Madison, USA, 2004.

[10] T. A. Lipo, **Introduction to AC Machine Design.** Wisconsin Power Electronics Research Center, University of Wisconsin, 2004.

[11] M. Liwschitz-Garik, C. C. Whiple, **Electric Machinery.** Vol. 2 AC Machines. Van Nostrand Publishers, 1961.

[12] P. L. Alger, **Induction Machines – Their Behavior and Uses.** Gordon and Breach Science Publishers, 1965.

[13] I. Mandić, **Computation of Magnetic Fields in Saturated Iron Structures with Special Reference to the Computation of Short Circuit Performance of Induction Motors with Wound Rotors.** Ph.D. thesis, University of Southampton, Faculty of Engineering and Applied science, Department of Electrical Engineering, Southampton, United Kingdom, 1974.

[14] D. Ban, D. Žarko, I. Mandić, **Turbogenerator End Winding Leakage Inductance Calculation Using a 3-D Analytical Approach Based on the Solution of Neumann Integrals.** IEEE Trans. on Energy Conversion, Vol. 20, No 1, pp. 98–105, March 2005.

Izračunavanje parametara motora s umetnutim permanentnim magnetima metodom konačnih elemenata. Prikazana je metoda proračuna parametara motora s umetnutim permanentnim magnetima u bilo kojoj radnoj točki korištenjem dvodimenzionalne metode konačnih elemenata. Metoda je prilagođena korištenju u fazi projektiranja motora gdje je potrebno odrediti parametre motora, posebice induktivitete, koji su istovremeno funkcija geometrijskih dimenzija motora i ograničenja naponskog izvora napajanja. Za proračun reaktancije glava namota korištena je analitička metoda bazirana na trodimenzionalnom modelu čeonog prostora motora u kojem je svaki svitak modeliran kao skup međusobno povezanih tankih ravnih linija. Proračun međuinduktiviteta svitaka u glavi namota baziran je na rješenju Neumannovog integrala. Navedeni pristup proračunu parametara je primijenjen na motoru s umetnutim magnetima snage 1,65 kW za koji je napravljen i ispitan prototip.

Ključne riječi: motor s permanentnim magnetima, induktiviteti, metoda konačnih elemenata, simulacija, ispitivanje

AUTHORS' ADDRESSES

Dr. sc. Damir Žarko
Prof. dr. sc. Drago Ban
University of Zagreb
Faculty of Electrical and Engineering and Computing
Department of Electrical Machines, Drives and Automation
Unska 3, 10000 Zagreb, Croatia

Ratko Klarić
Istarski vodovod d.o.o.
Sv. Ivan 8, 52420 Buzet, Croatia